Synchronization and spatiotemporal self-organization in the NO+CO reaction on Pt(100). I. Unsynchronized oscillations on the 1×1 substrate

Cite as: J. Chem. Phys. **100**, 8483 (1994); https://doi.org/10.1063/1.466746
Submitted: 08 September 1993 • Accepted: 16 February 1994 • Published Online: 31 August 1998

G. Veser and R. Imbihl

Synchronization and spatiotemporal self-organization in the NO+CO reaction on Pt(100). I. Unsynchronized oscillations on the 1×1 substrate

G. Veser and R. Imbihl
Fritz-Haber Institut der Max Planck Gesellschaft, Faradayweg 4-6, D 14195 Berlin, Germany

(Received 8 September 1993; accepted 16 February 1994)

The oscillatory NO+CO reaction on Pt(100) has been investigated in the 10^{-6} mbar range using photoemission electron microscopy (PEEM) as a spatially resolving method. The existence ranges for kinetic oscillations have been mapped out in (p_{CO},T)-parameter space with fixed $p_{NO}=4\times10^{-6}$ mbar. Kinetic oscillations occur within a partial pressure range of $0.8<p_{NO}/p_{CO}<1.9$. In the lower lying of two temperature windows for oscillatory reaction behavior, the oscillations proceed unsynchronized on a 1×1 substrate without exhibiting macroscopic rate variations. Instead, one observes spatiotemporal pattern formation which has been studied in detail. These patterns are dominated by periodic wave trains, which become unstable at lower temperatures, giving rise to spiral waves and irregularly shaped reaction fronts. With decreasing temperature, the front velocity increases, while simultaneously the spatial periodicity of the wave trains becomes larger. In agreement with theoretical predictions by a three-variable model, the local oscillations terminate at the upper T boundary via a Hopf bifurcation and at the lower T boundary via a bifurcation of the saddle-loop type.

I. INTRODUCTION

The NO+CO reaction on Pt surfaces is both of technological importance because of the key role NO_x emission plays in air pollution and of interest with respect to the dynamic behavior it displays.[1,2] One finds explosive product formation (the so-called "surface explosion") in temperature programmed reaction (TPR) experiments, multistability, kinetic oscillations, and spatiotemporal pattern formation.[3–14] These phenomena have been investigated intensively in recent years on a Pt(100) surface, leading to the formulation of a mathematical model which could explain most of the experimentally observed features.[5,9–12] The essential driving force for the oscillations has been shown to lie in the autocatalytic feedback mechanism inherent to the vacancy requirement for NO dissociation.

Spatially resolved measurements, which were conducted with the recently developed photoelectron emission microscope (PEEM), revealed a variety of interesting features: the observation of propagating reaction fronts, the high structural sensitivity of the pattern forming processes, and the appearance of chemical turbulence due to the absence of an efficient synchronization mechanism.[7,8] These investigations have been conducted using a Pt single crystal of cylindrical shape as a catalyst, whose surface contains all orientations of the [001] zone. Although only the orientational range around (100) displayed oscillatory behavior, it was quite evident that spatiotemporal pattern formation was strongly influenced by the structural properties of the cylindrical surface. In particular, the continuously varying step density gave rise to a strongly anisotropic front propagation. Moreover, the high defect concentration on this surface strongly suppressed any regular pattern formation. For this reason, the spatially resolved measurements were continued with a plane Pt(100) surface.

As expected, the spatial patterns exhibit a much higher degree of regularity on the plane Pt(100) surface. Additionally, with this large uniformly reacting surface, the possibility of gas-phase coupling is introduced. It turns out that this mode is ineffective at lower temperatures, where the oscillations proceed on a 1×1 substrate, but gas-phase coupling becomes efficient at higher temperatures when the oscillations take place on a largely hex-reconstructed surface. One then observes sustained rate oscillations on a homogeneously reacting surface and a transition to spatiotemporal pattern formation associated with a collapse of the oscillation amplitude. The results of this study in which we investigated the oscillatory behavior at elevated temperature will be reported in the forthcoming, second part of this report.

Here, in the first part, we map out the existence ranges for oscillations in the NO+CO reaction and then focus entirely on the spatiotemporal pattern formation in the lower-lying temperature range for oscillations. We present the experimental results and compare them with the predictions of a mathematical model, which has already been set up during earlier investigations.[5,7–9] Although the model reproduces a number of features in good accordance with the experimental findings, several discrepancies exist which indicate that the model needs further improvements in order to achieve a really quantitative description of the reaction.

II. EXPERIMENT

The experiments were all carried out in a standard stainless steel ultrahigh vacuum (UHV) chamber of about 80 ℓ volume, which was operated as an isothermal, gradient free flow reactor. The chamber could be pumped down to a base pressure of $p\leqslant2\times10^{-10}$ mbar by a combination of a 360 ℓ/s turbomolecular pump, an ion getter pump, and a titanium sublimation pump. The system was equipped with facilities for low energy electron diffraction (LEED), Auger electron spectroscopy (AES), a Kelvin probe for work function mea-

 0021-9606/94/100(11)/8483/9/$6.00

surements, and two quadrupole mass spectrometers (QMS), one of which was differentially pumped, for measuring partial pressures under reaction conditions.

For PEEM measurements, UV light from a deuterium discharge lamp (30 W, Ealing) with a maximum emission between 5.2 and 6.2 eV photon energy could be focused into a spot of ≈ 1 mm^2 onto the single crystal.[14] The ejected photoelectrons were focused by the electrostatic three electron lens system of the PEEM and, after amplification by a channel plate electron multiplier, imaged onto a phosphorous screen. These images were then recorded with a CCD camera and stored on a video tape. This allows for an imaging of the work function distribution on the sample surface with a lateral resolution of ≈ 1 μm at the video frequency of 50 Hz. The microscope could be pumped differentially by a 170 ℓ/s turbomolecular pump, thereby reducing the pressure at the channel plate by roughly two orders of magnitude with respect to the pressure in the main chamber under reaction conditions.

The two Pt(100) samples (dimensions $\approx 5\times 5$ mm^2, ≈ 1 mm thickness) were cleaned by standard methods involving repeated cycles of oxidation and Ar ion sputtering prior to each experiment. For the experiments, high purity gases were used (purity—CO 4.7, NO 2.8, both LINDE), which were introduced into the chamber via a feedback controlled gas-inlet system, so that the partial pressures during the reaction could be kept constant within $\leq 1\%$ precision. The partial pressures given in this report have been corrected for the different ion gauge sensitivities of the respective gases, i.e., $S_{CO}/S_{N_2} = 1.0$ and $S_{NO}/S_{N_2} = 0.8$ were used as correction factors.

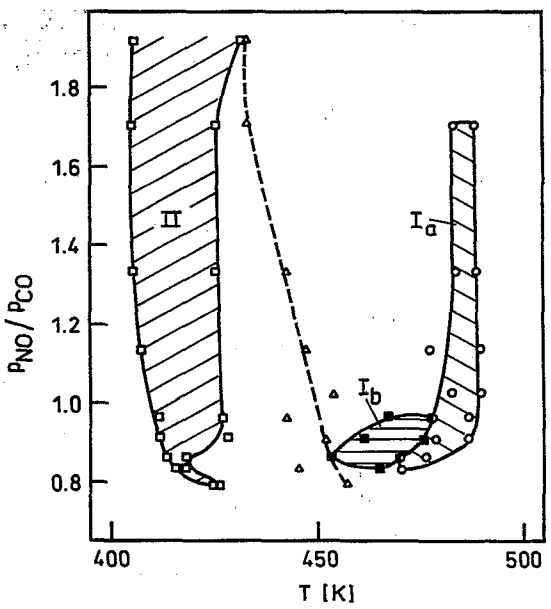

FIG. 1. Existence ranges for oscillatory behavior in the NO+CO reaction on Pt(100). Range Ia denotes the occurence of sustained rate oscillations, while ranges Ib and II mark spatiotemporal pattern formation, i.e., unsynchronized local oscillations without the occurrence of oscillations in the reaction rate. The existence ranges were determined on the cooling branch of a rate hysteresis with varying p_{CO} and with p_{NO} being kept fixed at $p_{NO}=4\times10^{-6}$ mbar. The dashed line marks the position of the "surface explosion" taking place on the heating branch of the rate hysteresis (see the triangles).

III. RESULTS

A. Existence range for oscillations

Figure 1 gives an overview of the two temperature ranges in which kinetic oscillations can be observed in the NO+CO reaction on Pt(100). The existence ranges had already been investigated with mass spectrometry in previous studies, where a small temperature jump (≈ 1–3 K) was used to excite oscillations.[5] This method yields only a very rough picture because the T pulse perturbs the system severely. Since PEEM, however, allows one to follow the oscillations on a local scale, it is no longer necessary to apply a synchronizing temperature jump in order to observe oscillatory behavior. The only severe limitation in PEEM measurements is the contrast, which may become very weak towards the boundaries of the existence range for oscillations.

By applying special care to the preparation of the sample, it was possible for the first time to obtain sustained oscillations in the upper temperature window, in contrast to earlier investigations, which had only reported damped oscillations in both windows. In the upper T window (range Ia), the oscillation range was therefore mapped out using measurements of the CO_2 production rate, while in the lower T window (range II), where the reaction rate is stationary, PEEM was used to follow the oscillations on a local scale. The oscillations in both T windows were recorded under constant partial pressure conditions on the cooling branch of a hysteresis that arises in a heating/cooling cycle.

Figure 1 displays two existence ranges for oscillations located at $T\approx 420$ and ≈ 485 K, which exhibit a width of ≈ 20 and ≈ 10 K, respectively. In range Ia, the rate oscillations proceed on a largely hex-reconstructed surface, while in range II, this reconstruction is completely lifted. One notes, that above $p_{NO}/p_{CO}=1$, the width and the location of both oscillatory windows is almost independent of the partial pressure ratio, i.e., the upper and lower T boundaries of the existence ranges are almost vertical. Below $p_{NO}/p_{CO}=1$ and adjacent to the low T boundary of range Ia, one finds a window (range Ib), in which spatiotemporal pattern formation occurs, but where the reaction rate is stationary.[12,13] The oscillatory behavior in this range is therefore analogous to the situation in the lower-lying T window for oscillations.

The comparison of this diagram with the results of earlier measurements shows that the main features are well reproduced, since one observes two T windows for oscillations whose width and separation along the T axis are nearly identical in the two investigations.[5] Only the location of the two T windows has been shifted by ≈ 30–50 K towards higher temperature as a consequence of the fact that we use partial pressures which are about one order of magnitude larger than in the earlier studies. One observes, however, some significant differences with respect to the partial pressure conditions under which kinetic oscillations occur. In contrast to earlier investigations in which rate oscillations could be excited for partial pressure ratios $4:3<p_{NO}/p_{CO}<3:1$, the existence range for oscillations now extends down to ratios

where p_{CO} is in excess, i.e., it extends over the partial pressure range $0.8<p_{NO}/p_{CO}<1.9$. The upper limit of 1.9 for oscillations in the lower T window presumably does not represent the true upper boundary for oscillations in range II, since this value just indicates the partial pressure value at which the contrast in the PEEM images became too low for the detection of oscillations. Yet, for range I, the ratio 1.9 represents the true upper limit for the rate oscillations.

B. Spatial pattern formation

Figure 2 displays a series of PEEM images showing different stages in the development of spatial patterns as the lower-lying existence range for oscillations (range II in Fig. 1) is traversed in the direction of decreasing temperature. This range is already located beyond the completion of the CO/NO-induced lifting of the hex reconstruction, i.e., the surface is in its (1×1) state. With decreasing temperature, the adsorbate coverage increases further until, finally, a state is reached where the NO dissociation and hence the overall reaction is inhibited. With respect to the reaction rate, the sequence of PEEM images therefore corresponds to a transition from a state of high reactivity to a state of low reactivity.

Coexisting with the reactive oscillatory state is an inactive state in which a high adsorbate coverage inhibits the reaction. The reaction is therefore bistable in the lower-lying existence range for oscillations, but the inactive state is metastable and undergoes a slow transition to the stable active state via nucleation of reaction fronts.[14] Depending on the heating rate which controls the degree of supersaturation, both heterogeneous and homogeneous nucleation of reaction fronts can be observed. Homogeneous nucleation manifests itself in the occurrence of a "surface explosion," i.e., a spike-like sudden rise of the reaction rate upon heating the catalyst, while heterogeneous nucleation can be observed to take place at defect sites on the surface.

In the following, we neglect the various aspects of front nucleation which have already been discussed in a separate publication[14] and focus onto the properties and the development of the regular wave trains. These are obtained by very slowly cooling the sample down to a certain temperature between ≈420 and 405 K and then keeping the temperature constant within ±0.1 K.

The first patterns that can be identified in PEEM are parallel wave trains with an extremely low contrast between the wave crests and the wave troughs, as demonstrated by Fig. 2(a). The waves have a wavelength of ≈29 μm and propagate at a velocity of ≈10 μm/s. The wave pattern exhibits a large number of dynamical defects as reaction fronts are broken apart and merge with other succeeding fronts. Thus, the maze-like pattern of Fig. 2(a) is created. The waves are being emitted from several trigger centers, one of which is visible in the upper left part of Fig. 2(a), and then seem to propagate preferentially along certain directions over the crystal. These directions are not aligned along the crystallographic axes, but presumably are defined by structural defects.

Upon subsequent lowering of the catalyst temperature, the wavelength and propagation velocity increase and the contrast becomes stronger. This is shown in Fig. 2(b)–2(g).

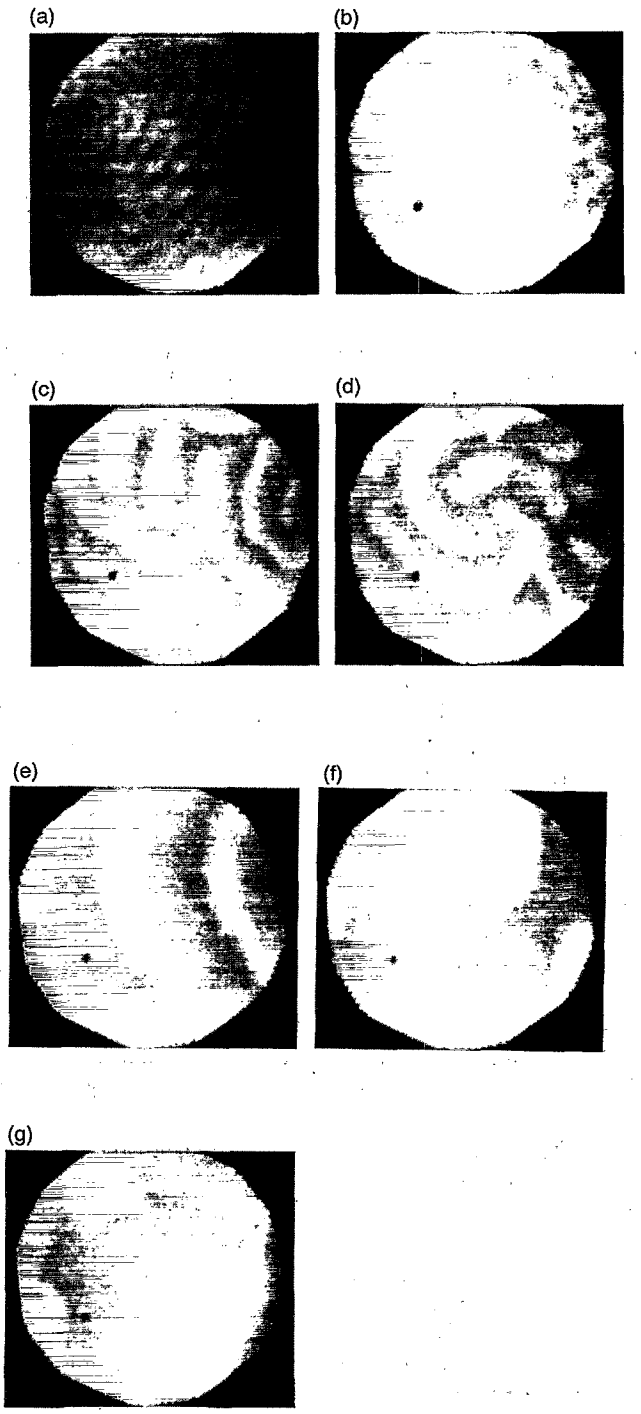

FIG. 2. PEEM images showing various stages in the development of spatial patterns as the existence range II for oscillations is traversed in the direction of decreasing temperature. The diameter of the depicted area is ≈500 μm. The experimental conditions were $p_{NO}=4\times10^{-6}$ mbar, $p_{CO}=2.8\times10^{-6}$ mbar, and T=(a) 421; (b) 419 K; (c) 417 K; (d) 415; (e) 413; (f) 410; and (g) 407 K.

Around $T=416$ K, the parallel reaction fronts become unstable and spiral waves are formed. These spirals typically do not develop more than one or two windings before they are disrupted by other reaction fronts. Sometimes, two- and three-armed spirals are formed, examples of which are dis-

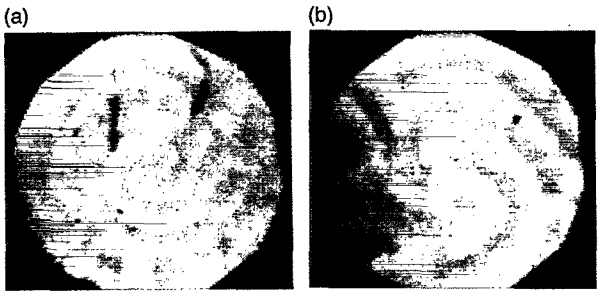

FIG. 3. PEEM images showing two- and three-armed spirals. The diameter of the depicted area is ≈500 μm. The experimental conditions were $p_{NO}=4\times10^{-6}$ mbar, $p_{CO}=2.4\times10^{-6}$ mbar, and T=(a) 416.5 and (b) 415 K.

played in Fig. 3. These multiarmed spirals, however, are not stable, but always decompose into an equivalent number of independent spirals. One of these single-armed spirals then stays pinned to the original location of the multiarmed spiral, while the other(s) slowly drift away.

Below a temperature of about 410 K, the wavelength of the pattern becomes of the order of the diameter of the PEEM images, which due to instrumental limitations could not be made larger than ≈500 μm. The reaction fronts become ragged, as can be seen in Fig. 2(f). This raggedness arises due to the fact that the fronts no longer exhibit a uniform propagation velocity, but certain sections slow down in some areas of the crystal, while elsewhere others speed up. This uneven propagation leads to strongly curved reaction fronts, which then very often break apart in this process. This instability gets stronger with decreasing temperature, until, just before the whole catalyst surface becomes inactive, no waves are formed any more, but only irregular reaction pulses are emitted aperiodically from some defect areas. A PEEM image showing this type of behavior is displayed in Fig. 2(g).

In the course of this whole development, the reaction rate decreases continuously and, accordingly, the mean brightness of the images decreases. In parallel, the contrast in the pictures greatly enhances, corresponding to an increase in the amplitude of the local oscillations. A quantitative evaluation of the PEEM images discussed above is given in Figs. 4–6. The temperature dependence of the front propagation velocity c is reproduced in Fig. 4(a) while Fig. 4(b) displays the corresponding variation in the spatial wavelength of the wave trains. The velocity c varies between 10 and 25 μm/s, which is about the velocity range which is typically found in low pressure single crystal experiments.[7,15,16] Surprisingly, however, the velocity *increases* with decreasing temperature, a behavior which so far has not been found in other surface reactions. The wavelength of the wave trains comprises a range from ≈30 to 400 μm in the T range from 407 to 421 K, increasing practically monotonically with decreasing T as demonstrated in Fig. 4(b).

Since the increase of the wavelength is much stronger than that of the wave velocity, the local oscillation frequency, which is just the quotient of wave velocity over wavelength, consequently decreases. The resulting temperature dependence of the oscillation frequency ν_{local} is displayed in Fig. 5.

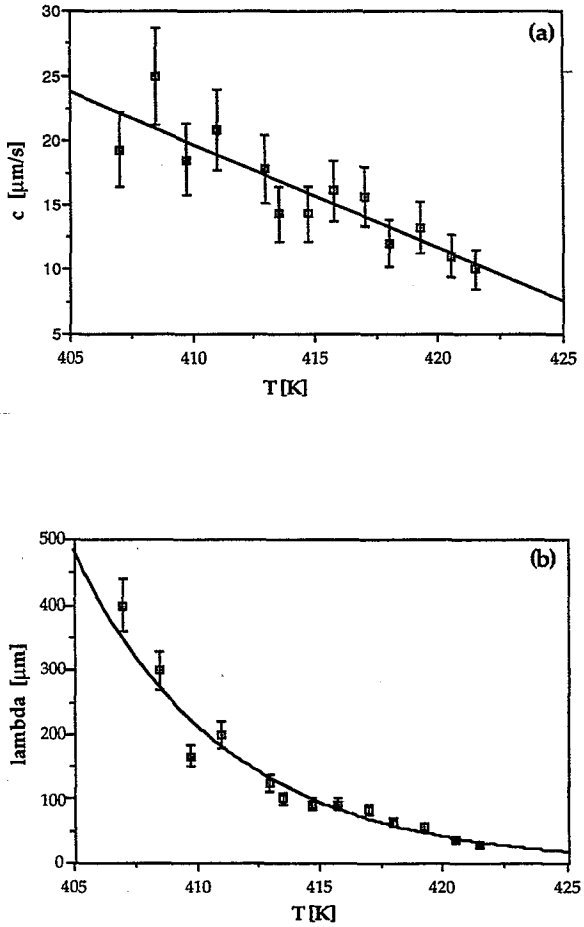

FIG. 4. Temperature dependence of (a) the front velocity and (b) the spatial periodicity of periodic wave trains in range II. The experimental conditions were $p_{NO}=4\times10^{-6}$ mbar and $p_{CO}=2.8\times10^{-6}$ mbar.

The local oscillation frequency is about 0.3 Hz at 422 K and then falls monotonically to 0.05 Hz at 407 K. It should be added that irrespective of whether ν_{local} is calculated with $\nu_{local}=c/\lambda$, or measured directly by integrating the PEEM intensity in a small window of 20×20 μm size, both values agree within 10% accuracy, thus demonstrating the regular behavior of the wave trains.

The same diagram (Fig. 5) also exhibits the variation of the oscillation amplitude as determined from the local variation of the PEEM intensity. The behavior of the amplitude is contrary to that of the frequency. The oscillations start with a small amplitude which then increases monotonically with decreasing T. At the low T boundary of the oscillatory range, the oscillation amplitude collapses in a discontinuous transition. As mentioned above, the increase in the oscillation amplitude with decreasing temperature takes place superimposed on a decreasing brightness of the PEEM image. This relation is illustrated by Fig. 6, where the local PEEM intensity at the upper and the lower turning points of the oscillations has been plotted. The information contained in the PEEM intensity is the local work function, which in turn depends on the adsorbate coverages. Evidently, the adsorbate coverage during the oscillations increases with decreasing

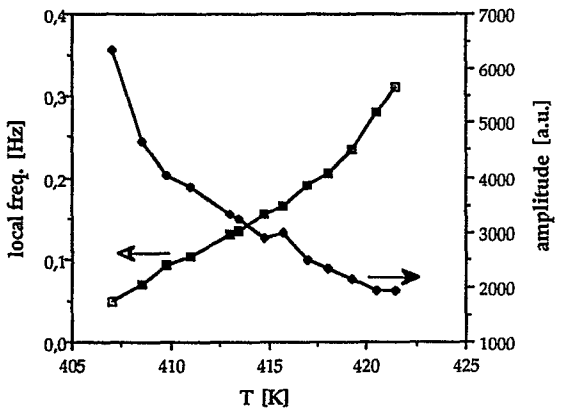

FIG. 5. Temperature dependence of the frequency and amplitude of local oscillations in range II as measured via PEEM. The experimental conditions were $p_{NO}=4\times10^{-6}$ mbar and $p_{CO}=2.8\times10^{-6}$ mbar.

temperature. Furthermore, the state of an adsorbate free surface is apparently not reached under oscillatory conditions. One also notes that the mean intensity in the PEEM images follows quite closely the steep decrease of the oscillation minima, while the maximum intensity displays a much shallower slope. This dependence is a consequence of the shape of the front profile, as will be shown further below.

The interpretation of the different gray levels seen in the PEEM images is not trivial in the NO+CO reaction, since both atomic oxygen and CO cause similarly strong work function increases of ≈400 and ≈250 mV, respectively.[17–21] On the other hand, molecularly adsorbed NO causes only a small $\Delta\phi$ decrease of 50 mV at a maximum below the level of the clean hex surface.[21] The bright areas in the PEEM images could therefore be either associated with a NO covered or a largely adsorbate free 1×1 surface. However, Fourier-transform infrared (FTIR) measurements of the NO+CO reaction on Pt(100)-1×1 have shown that the maximum in the reaction rate correlates with the maximum

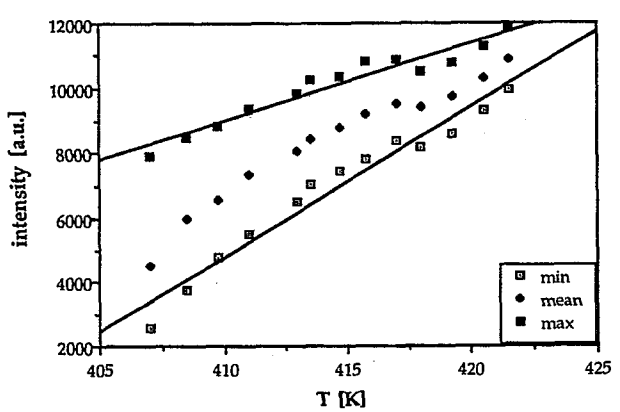

FIG. 6. A plot showing the upper and lower turning points of local oscillations as measured through the PEEM intensity integrated in a window of ≈20×20 μm^2 size. The filled squares in between the two extrema denote the temporal average of the local oscillations. The experimental conditions were $p_{NO}=4\times10^{-6}$ mbar and $p_{CO}=2.8\times10^{-6}$ mbar.

in NO coverage.[22] Since, additionally, PEEM demonstrates that during the occurrence of the "surface explosion" an increasing CO_2-production rate is accompanied by an increasing intensity, we can assign the bright areas in the images to a NO covered surface with a possible contribution of some adsorbate free 1×1 surface.

Accordingly, the dark area can be associated with a CO covered surface. This interpretation is supported by small-area LEED measurements (electron beam diameter ≈20 μm) conducted by Swiech *et al.*[23] Their measurements showed that during the passage of a reaction front in the oscillatory range II, the LEED pattern changes from a diffuse $c(4\times2)$ to a diffuse $(\sqrt{2}\times3\sqrt{2})R45°$ structure. Assigning these two patterns to NO covered and CO covered surfaces, respectively, this means that the coverage in an oscillatory cycle changes from $\Theta_{CO}\approx0.67$ to $\Theta_{NO}\approx0.5$. With the above given interpretation, the contribution of atomic oxygen to the gray levels seen in PEEM remains to be specified. The simplest assumption that is consistent with the available experimental data would be that the oxygen coverage is always so small that it does not contribute substantially to the PEEM intensity. Thus, the coverage in an oscillatory cycle would essentially vary between a CO covered (dark) and an NO covered (bright) surface. From the reaction mechanism, one can conclude that at some stage a largely adsorbate-free 1×1 surface should also exist. How large the contribution of this phase actually is, however, remains to be specified.

Profiles of the reaction front at varying temperatures are displayed in Fig. 7. The shape changes from a harmonic profile at high temperatures to a strongly anharmonic, triangular profile at lower T. At low temperature, a new, step-like feature of ≈10–20 μm width develops in the steep flank of the profile. One could suspect that the plateau indicates the presence of a certain well-defined adsorbate phase. Using the work function data available in the literature, however, an assignment is a rather difficult task. Due to the simultaneous presence of a linear- and a bridge-bonded species in CO/Pt(100), the dependence of the work function on the CO coverage is not simple, but depends on the preparation of the CO adlayer.[17,18,24]

Local time series, corresponding to the profiles shown in Fig. 7, display the same characteristics, i.e., relaxational type oscillations at low temperature and sinusoidal oscillations at high temperature. The simple type of local oscillations, which corresponds to the regular wave trains, changes towards the low-T boundary of the oscillatory range. One then observes sequences of regular oscillations followed by relaxational type oscillations with irregularly varying length, as depicted in Fig. 8. As shown in this plot, these oscillations involve essentially three different intensity levels, with the lowest one being associated with an adsorbate poisoned surface, i.e., with a high adsorbate coverage inhibiting NO dissociation.

One characteristic feature of the NO reduction reactions found in previous investigations is the extreme sensitivity of these reactions to the imperfections of the surface structure.[7,16] This characteristic of the NO+CO reaction also becomes apparent in the present investigation, as shall be demonstrated by three examples. As outlined above, struc-

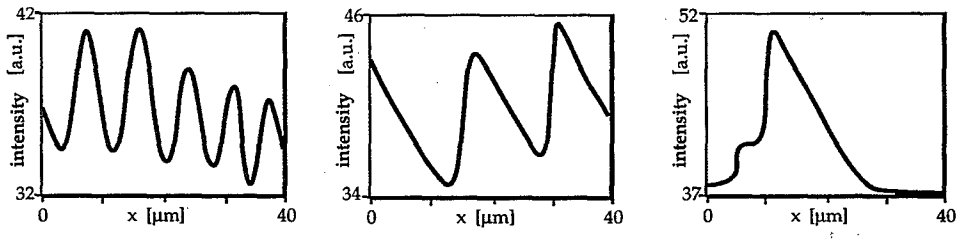

FIG. 7. PEEM intensity profiles of reaction fronts showing the transition from a harmonic profile at higher T [(a) $T=418$ K] to a relaxational type profile at lower T [(b) $T=413$ K] and finally the appearance of a step-like feature in the front profile [(c) $T=407$ K]. The reaction front in all three plots is moving from right to left. The experimental conditions were $p_{NO}=4\times10^{-6}$ mbar and $p_{CO}=2.8\times10^{-6}$ mbar.

tural imperfections act as nuclei for the formation of reaction fronts during the transition from the inactive metastable branch to the stable active branch.[14] Two PEEM images showing heterogeneous front nucleation at a large defect upon slowly heating up the sample to ≈417 K are displayed in Fig. 9. Interestingly, the reaction fronts that are formed first are aligned parallel to one another, while the wave pattern subsequently becomes rather irregular as more and more waves are being emitted by the defect. A completely different kind of defect disturbing the formation of regular wave patterns is shown in the PEEM image in Fig. 10(a). One can make out two perfectly straight, thin lines, which separate reaction fronts propagating in opposite directions (the "head" of the front is always bright, while the tail is dark). These lines have a width which is just resolvable in PEEM, i.e., of ≈1–5 μm. Since polishing scratches are usually not as sharp and as perfectly straight as these lines, we assume that they represent dislocations or step bundles.

An observation that demonstrates the sensitivity of the NO+CO reaction even to microscopic defects is depicted in the PEEM image in Fig. 10(b). This image was taken from an area quite close to the rim of the crystal. No parallel waves are formed any more, but only patterns with very rough reaction fronts cover the area. For comparison, Fig. 2(c) shows the same type of pattern, but in an area further away from the rim. Since the surface structure close to the rim exhibits more structural imperfections than the rest of the catalyst surface, this behavior can be assigned to surface defects. However, since we could not resolve any macroscopic (≥1 μm) defects in this area with PEEM, we attribute the cause of the front roughening to microscopic defects. This hypothesis was tested by sputtering the crystal for a few minutes without subsequent annealing. Exactly the same kind of rugged pattern formation as shown in Fig. 10(b) was found all over the surface. Therefore, we can definitely attribute the raggedness to microscopic defects of the surface structure.

Finally, a quite curious phenomenon has been observed in the experiments at very low temperatures ($T\approx405$ K) when the reaction had almost completely been suppressed by an increasing adsorbate coverage. While at these low temperatures no product formation was detectable with QMS in the gas phase, in PEEM a few active spots were still visible on the surface. The PEEM image in Fig. 11 displays such an active spot where a reactive pulse was constantly and very regularly traveling in a circle around a small area of about

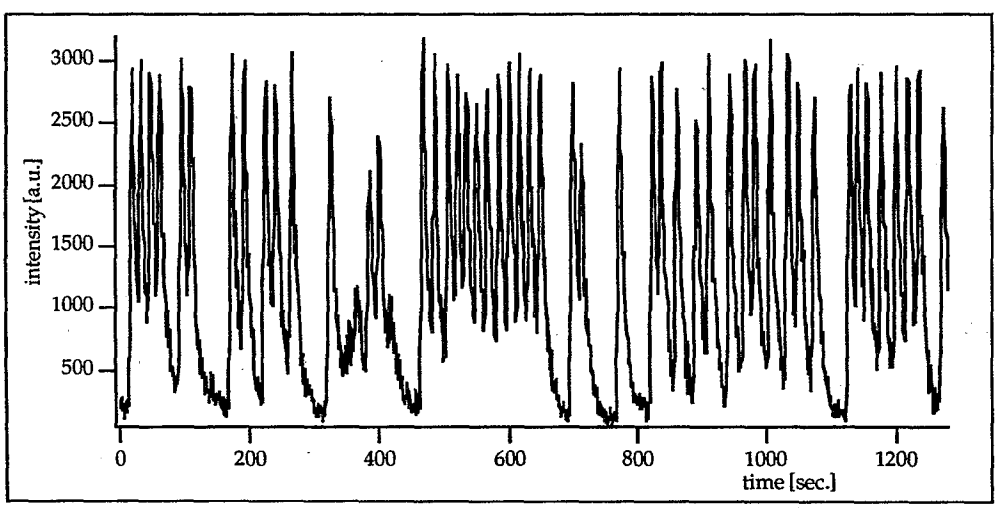

FIG. 8. Local time series showing irregular intensity oscillations occurring close to the saddle-loop bifurcation at the low-T end of the existence range for oscillations. The experimental conditions were $p_{NO}=4\times10^{-6}$ mbar, $p_{CO}=2.1\times10^{-6}$ mbar, and $T=406$ K.

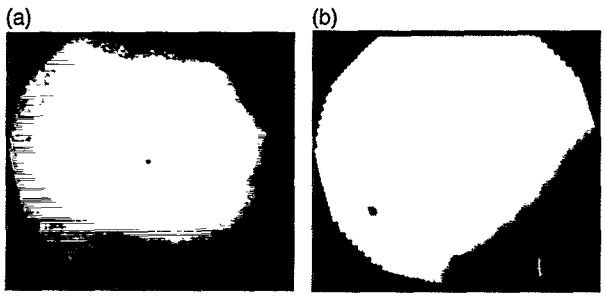

FIG. 9. PEEM images showing heterogeneous nucleation of reaction fronts at a large defect upon heating the sample to ≈417 K. While the first waves that are formed are very regular (a), this regularity is lost during the further propagation of these reaction fronts (b). The experimental conditions were $p_{NO}=4\times10^{-6}$ mbar and $p_{CO}=2.5\times10^{-6}$ mbar.

$100\times50\ \mu m^2$. The path of the pulse must apparently be determined by some surface defects which were sufficiently active to retain some reactivity. The pulsating pattern was able to survive down to temperatures several degrees Kelvin lower than the reactivity of the rest of the surface area.

IV. DISCUSSION

A. A comparison with the three-variable model

For the NO+CO reaction on Pt(100), a mathematical model has been developed based on the vacancy mechanism for NO dissociation and on the $1\times1 \leftrightarrow$ hex surface phase transition, which correctly reproduces the hysteresis behavior of the reaction and the two existence ranges for oscillations.[5,9] By keeping the surface frozen in a 1×1 configuration, this six-variable model could be reduced to only three equations which were then analyzed with bifurcation theory.[9] Since the model uses only ordinary differential equations, it describes the behavior of an individual oscillator, and the simulation results should therefore be comparable to the local measurements with PEEM in the lower-lying existence range for oscillations.

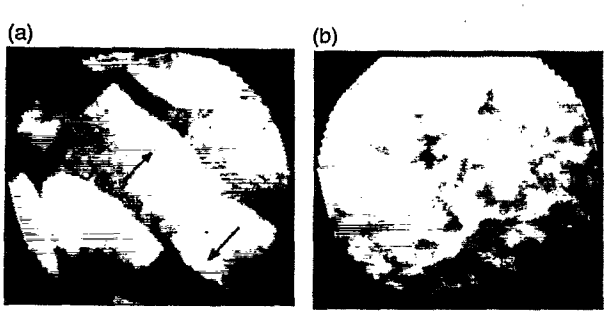

FIG. 10. The influence of surface defects on spatial pattern formation in the NO+CO reaction. (a) The PEEM image showing three wave trains which are separated by two thin lines (presumably dislocations) in the lower and upper thirds of the image. The waves are traveling in opposite directions as indicated by the arrows. The experimental conditions were $p_{NO}=4\times10^{-6}$ mbar, $p_{CO}=3.0\times10^{-6}$ mbar, and $T=413$ K. (b) The formation of a rough wave pattern recorded close to the edge region of the single crystal surface. The experimental conditions were $p_{NO}=4\times10^{-6}$ mbar, $p_{CO}=2.6\times10^{-6}$ mbar, and $T=417$ K.

FIG. 11. PEEM image showing a single pulse traveling periodically on a closed loop of ~100 μm diameter while surrounded by an unreactive medium. The experimental conditions were $p_{NO}=4\times10^{-6}$ mbar, $p_{CO}=2.3\times10^{-6}$ mbar, and $T=403$ K.

The present investigation yields an existence range for oscillations on Pt(100)-1×1 which extends from 405 to 430 K in the 10^{-6} mbar range and comprises partial pressure ratios from $p_{NO}/p_{CO}\approx1.9$ down to ≈0.8. With respect to earlier investigations, the main new result of the present investigation is that the oscillatory range now also extends to conditions where CO is in excess. The three-variable model, in addition to a large oscillatory window which ranges from the stochiometric 1:1 ratio up to $p_{NO}/p_{CO}=1.6$, also yields a second window in which oscillatory behavior is found with CO being in excess. However, in the bifurcation diagram in (p_{NO},T)-parameter space, this second window, which comprises a partial pressure range of $0.93<p_{NO}/p_{CO}<1$, is much smaller than in the experiment and, most importantly, the experiments give no indication that the oscillatory range is split into two distinct parts. Clearly the mathematical model does not correctly reproduce the experimental bifurcation behavior in the parameter range where CO is in excess.

With regard to the width of the oscillatory temperature range and the bifurcation behavior at the upper and lower T boundaries, the PEEM results fit very well into the predictions of the model. The bifurcation analysis yields a Hopf bifurcation (HB) at the upper T boundary and a saddle loop (SL) bifurcation at the lower boundary.[9] Experimentally, the oscillations start with a small amplitude at the upper T boundary (see Fig. 5) and the transition from steady state behavior to oscillations is not associated with a hysteresis, which is consistent with a (supercritical) Hopf bifurcation. Additionally, near the onset of the local oscillations, i.e., between ≈415 and 421 K, the oscillation amplitude follows closely a square-root dependence with respect to the distance $|\mu-\mu_c|$ from the bifurcation point at μ_c. Such a scaling law is predicted in the vicinity of a Hopf bifurcation. By extrapolating the data points between ≈415 and 421 K, we can determine the critical temperature of the Hopf bifurcation T_{HB} to be $T_{HB}\approx424.3\pm0.3$ K.

At the lower T boundary, the PEEM results fit very well into the SL bifurcation predicted by the three variable model. Towards the bifurcation point, the period of the oscillations increases exponentially and the oscillation amplitude collapses in a discontinuous transition at the critical point. Additionally, we can clearly discriminate between the SL bifurcation and a saddle node with infinite period (SNIPER)

bifurcation. First, in a SL bifurcation, the period increases exponentially towards the critical bifurcation point at μ_c, while in a SNIPER, the period τ_{osc} follows a dependence $\tau_{osc} \sim 1/\sqrt{|\mu_c - \mu|}$.[25] Using the data points from Fig. 5 between $T \approx 415$ and 407 K, we found that an exponential, i.e., a SL-type dependence of the period, yields a better fit to the data than the dependence predicted by a SNIPER bifurcation (the correlation of the data is 0.995 in the first case and 0.989 in the second). Moreover, the existence of a hysteresis as was found in these experiments would be inconsistent with a SNIPER bifurcation, since with this type of bifurcation, the stable focus arises exactly on the limit cycle. From the temperature dependence of the oscillation period, we extrapolate the critical temperature T_{SL} for SL to $T_{SL} \approx 406.3 \pm 0.1$ K.

B. Spatial pattern formation

The various types of chemical waves which have been seen in this study, i.e., periodic wave trains, spiral waves, and pulses, have been observed in other oscillatory surface reactions as well and, quite generally, these structures represent solutions of reaction-diffusion systems.[15,16,26] What is unique in the NO+CO reaction on Pt(100)-1×1 is that gas-phase coupling apparently provides no synchronizing effect for the local oscillators as evidenced by the absence of sustained rate oscillations. One would suspect that the inefficiency of gas-phase coupling is just a consequence of too low an amplitude of the partial pressure variations, which are of the order of ≈1%. Experiments with a strongly reduced pumping rate demonstrated, however, that even with the amplitude reaching ≈15%–20%, no efficient synchronization can be achieved.

Evidently, the reason for the lack of synchronization has to be sought in the system itself, i.e., in the feedback mechanism between partial pressure variations and their influence on the surface reaction. Quite generally, it has been shown that depending on the reaction system, global coupling can either have a stabilizing or a destabilizing effect on the spatial homogeneity.[27] How this analysis, which has been conducted with the complex Ginzburg–Landau equation, modified to take into account the effect of global coupling applies to the NO+CO reaction on Pt(100), however, remains to be worked out in detail.

The existence of chemical waves and pulses in the NO+CO reaction has been demonstrated in 1D simulations by Evans *et al.*[10] By adding appropriate terms for NO and CO diffusion to the equations of the three-variable model, they transformed the ordinary differential equations (ODEs) into a system of partial differential equations (PDEs). Neglecting oxygen diffusion and assuming equal diffusion constants for NO and CO, the experimentally determined front velocity of ≈17.5 μm/s at 413 K allows one to estimate the NO and CO diffusion constants to be $D_{NO} = D_{CO} = 1.9 \times 10^{-5}$ cm^2/s. What appears to fit very well into the experimental observation of periodic wave trains is that, starting with a single planar interface between an adsorbate free and an adsorbate covered surface, periodic wave trains were obtained in the 1D simulations. This behavior is somewhat unusual, since in most cases periodic wave trains are only obtained if a trigger center periodically emits waves. In the present system, however, the formation of these periodic wave trains appears to be an inherent property of the coupling between reaction and diffusion.

The damping effect in the oscillation amplitude, which has been observed after exciting rate oscillations with a small T jump (≈1–3 K), can be attributed to these periodic wave trains. After the T jump, the system is in an unsynchronized, i.e., spatially more or less homogeneous state, and one observes macroscopic rate oscillations.[5,6] However, as periodic waves trains form and spread out, finally covering the whole surface area, the rate oscillations decay and a stationary rate is reached. This effect has been demonstrated in 2D simulations by Yelenin *et al.*, who also used the three-variable model complemented by CO and NO diffusion terms.[11]

In both simulations by Yelenin *et al.* as well as in those by Evans *et al.*, it was also shown that Turing patterns arise if the difference in the diffusion constants of CO and NO become sufficiently large, i.e., if D_{CO} and D_{NO} differ by more than a factor of 10. The fact that no Turing patterns were detected experimentally could thus be taken as an indication that NO and CO diffuse about equally fast on Pt(100)-1×1 as suggested by their similar adsorption energy.[18,28]

The chemical waves in the NO+CO reaction exhibit one rather unusual property, which is their *increasing* velocity with decreasing temperature. Since all rate constants which could play a role decrease with decreasing temperature, there is no simple explanation for this unusual dependence. In order to solve this problem, a starting point would again be the three-variable model to see whether it can reproduce this behavior. Already the short analysis of this system conducted by Evans *et al.* revealed that the three-variable model exhibits a number of unusual properties which are profoundly different from the properties of pulses and wave propagation in the catalytic CO oxidation on Pt surfaces.[10]

Comparing our present results, which were obtained on a flat Pt(100) single crystal, to previous investigations which were performed on a cylindrical single crystal (axis ∥ [001]),[7,8] we note some significant differences, although the main conclusions are identical. Both studies show that at lower temperatures, the surface only oscillates on a local scale, thus explaining the absence of sustained rate oscillations in the low temperature window. On both surfaces, one observes periodic wave trains, but on the flat Pt(100) sample, the patterns exhibit a much higher degree of order. Rotating spirals as well as nicely aligned parallel wave trains have only been found on the flat sample, but not on the Pt cylinder. The cylinder surface does not exhibit large flat areas, but on the other hand, many structural heterogeneities such as atomic steps and facets are present.

In contrast to the Pt cylinder, no turbulent wave patterns have been found on the flat Pt(100) surface. As demonstrated by Fig. 2, some mild disorder is also present in the periodic wave trains on Pt(100). This disorder, which is dynamic and not static, can most likely also be explained by the effect of structural imperfections. The defects cause the breaking of the planar wave front, and as the free ends form new connections with other wave fronts, dynamical dislocations are

constantly created and removed. The dynamics and statistics of these processes is probably an interesting subject to study since one should expect that some of the concepts well known from defects in solid state matter should also be applicable to the regular wave patterns.[29]

V. CONCLUSIONS

The NO+CO reaction exhibits oscillatory behavior on Pt(100) in two separate temperature ranges within a partial pressure range $0.8<p_{NO}/p_{CO}<1.9$. In the lower-lying existence range, no macroscopic rate oscillations are found. Instead, spatiotemporal pattern formation is observed on the catalyst surface. These patterns are dominated by the presence of periodic wave trains. The spatial wavelength and the front velocities of these wave trains have been found to increase with decreasing temperature. The experimentally determined bifurcation behavior at the boundaries of the oscillatory T range agrees with the predictions of the three-variable model for the NO+CO reaction—a Hopf bifurcation at the upper T boundary and a SL bifurcation at the lower T boundary could clearly be identified. Although some features are well reproduced, the comparison of the experimental results with the predictions of the three-variable model reveals a number of shortcomings of the model, which needs to be improved further for a quantitative and qualitative description of the NO+CO reaction on Pt(100)-1×1.

ACKNOWLEDGMENTS

Technical assistance by S. Wasle is gratefully acknowledged. The authors thank Dr. C. S. Rastomjee for carefully reading the manuscript. G. V. thanks the "Stiftung Stipendienfonds des VCI" for support through a Kékulé scholarship.

[1] H. Bosch and F. Janssen, Catal. Today **2**, 369 (1988).
[2] W. F. Egelhoff, in *The Chemical Physics of Solid Surfaces and Heterogeneous Catalysis*, edited by D. A. King and D. P. Woodruff (Elsevier, Amsterdam, 1982), pp. 401.
[3] S. P. Singh-Boparai and D. A. King, in Proceedings of the 4th International Congression Surface Science, Cannes, 1980, pp. 403.
[4] S. B. Schwartz and L. D. Schmidt, Surf. Sci. **206**, 169 (1988).
[5] T. Fink, J.-P. Dath, R. Imbihl, and G. Ertl, J. Chem. Phys. **95**, 2109 (1991).
[6] J.-P. Dath, T. Fink, R. Imbihl, and G. Ertl, J. Chem. Phys. **96**, 1582 (1992).
[7] G. Veser and R. Imbihl, J. Chem. Phys. **96**, 7155 (1992).
[8] G. Veser and R. Imbihl, Surf. Sci. **269/270**, 465 (1992).
[9] R. Imbihl, T. Fink, and K. Krischer, J. Chem. Phys. **96**, 6236 (1992).
[10] J. W. Evans, H. H. Madden, and R. Imbihl, J. Chem. Phys. **96**, 4805 (1992).
[11] G. G. Yelenin and A. G. Makeev, Math. Modeling (in Russian) **4**, 5 (1992).
[12] G. Veser, F. Mertens, A. Mikhailov, and R. Imbihl, Phys. Rev. Lett. **71**, 935 (1993).
[13] G. Veser and R. Imbihl, J. Chem. Phys. **100**, 8492 (1994).
[14] G. Veser, P. A. Thiel, and R. Imbihl, J. Phys. Chem. **98**, 2148 (1994).
[15] S. Jakubith, H. H. Rotermund, W. Engel, A. von Oertzen, and G. Ertl, Phys. Rev. Lett. **65**, 3013 (1990).
[16] G. Veser, F. Esch, and R. Imbihl, Catal. Lett. **13**, 371 (1992).
[17] R. J. Behm, P. A. Thiel, P. R. Norton, and G. Ertl, J. Chem. Phys. **78**, 7437 (1983).
[18] P. A. Thiel, R. J. Behm, P. R. Norton, and G. Ertl, J. Chem. Phys. **78**, 7448 (1983).
[19] K. Griffiths, T. E. Jackman, J. A. Davies, and P. R. Norton, Surf. Sci. **138**, 113 (1984).
[20] P. Gardner, R. Martin, M. Tüshaus, and A. M. Bradshaw, J. Electron Spectrosc. Relat. Phenom. **54/55**, 619 (1990).
[21] T. Fink, J.-P. Dath, M. R. Bassett, R. Imbihl, and G. Ertl, Surf. Sci. **245**, 96 (1991).
[22] P. Gardner, R. Martin, R. Nalezinski, and A. M. Bradshaw (unpublished).
[23] W. Swiech and S. Rastomjee (private communication).
[24] J. E. Jackman, K. Griffiths, J. A. Davies, and P. R. Norton, J. Chem. Phys. **79**, 3529 (1983).
[25] J. M. T. Thompson and H. B. Stewart, *Nonlinear Dynamics and Chaos* (Wiley, New York, 1987).
[26] A. S. Mikhailov, *Foundations of Synergetics* (Springer, Berlin 1991).
[27] F. Mertens, R. Imbihl, and A. S. Mikhailov, J. Chem. Phys. **99**, 8668 (1993).
[28] R. J. Gorte, L. D. Schmidt, and J. L. Gland, Surf. Sci. **109**, 367 (1981).
[29] P. Manneville, *Dissipative Structures and Weak Turbulence* (Academic, San Diego, 1990).